PHYSICAL REVIEW E, VOLUME 64, 016214

Chaotic behavior in lemon-shaped billiards with elliptical and hyperbolic boundary arcs

V. Lopac

Division of Physics, Faculty of Chemical Engineering and Technology, University of Zagreb, Zagreb, Croatia

I. Mrkonjić and D. Radić

Department of Physics, Faculty of Sciences, University of Zagreb, Zagreb, Croatia

(Received 18 December 2000; revised manuscript received 28 February 2001; published 19 June 2001)

Chaotic properties of a new family, ellipse hyperbola billiards (EHB), of lemon-shaped two-dimensional billiards, interpolating between the square and the circle, whose boundaries consist of hyperbolic, parabolic, or elliptical segments, depending on the shape parameter δ, are investigated classically and quantally. Classical chaotic fraction is calculated and compared with the quantal level density fluctuation measures obtained by fitting the calculated level spacing sequences with the Brody, Berry-Robnik, and Berry-Robnik-Brody distributions. Stability of selected classical orbits is investigated, and for some special hyperbolic points in the Poincaré sections, the ''blinking island'' phenomenon is observed. Results for the EHB billiards are compared with the properties of the family of generalized power-law lemon-shaped billiards.

DOI: 10.1103/PhysRevE.64.016214 PACS number(s): 05.45.−a, 03.65.−w

I. INTRODUCTION

Among various systems exhibiting chaotic behavior, the two-dimensional planar billiards occupy a special place. They provided examples of chaotic behavior in the low-dimensional classical Hamiltonian systems [1–3]. They also played a crucial role in extending the subject of chaos to quantum mechanics [4–6]. In the great majority of billiards investigated in the literature, the boundaries consist of circular arcs [1,7–10], or are obtained by a conformation of the circle [11–15]. Recent works examine the effects of singular points in the boundary [10], the exotic boundary shapes [16–18], the three-dimensional billiards [19], and the comparison between the quantal, classical, and semiclassical solutions of the billiard problem [20–26].

A large amount of theoretical results on closed billiards is devoted to the understanding of orbits and their stability. The particle moves within the boundary and exhibits specular reflections on the billiard wall, with no additional forces present. The only integrable billiard of this type is the full ellipse, including the circle [1]. At the other extreme are billiards that exhibit fully chaotic (ergodic) behavior, represented by the Bunimovich (stadium) billiard [2], the Sinai billiard [3], and, according to the numerical evidence, the Robnik billiard [12] for some specific parameter choices. Between these two extremes, depending on the billiard shape and on the initial conditions, the behavior can be regular, quasiregular [in the sense of the (KAM) theorem] or chaotic. Some results on the pseudointegrable (triangular, quadrangular, polygonal) and integrable billiards are reported in Refs. [27–31]. Planar billiards containing a particle in the magnetic field, or equivalently, the free particle motion in a rotating billiard, have been analyzed in [32–36].

Other types of billiards have attracted attention in recent years. These are the open billiards in the vertical plane, where the particle submitted to the constant gravitational field bounces elastically off the billiard walls. The best-known billiard of this type is the wedge billiard [37–40], which revealed complicated variations of dynamics, known as the ''breathing chaos,'' when the wedge angle is varied [41]. More recently, other gravitational billiards with different wall shapes have been reported [42,43]. The gravitational billiard with the parabolic well [42] is fully integrable, and this is the only known example of an integrable billiard besides the closed elliptical billiard. The most conspicuous property of the wedge billiard is the existence, in the phase plane, of singular regions, which cannot be described by the KAM theorem. Similar singularities occur also in other low-dimensional dynamical systems [44]. Generally, the extent of chaos and the character and stability of classical orbits in billiards are determined by the analytic form of the boundary segments, the continuity or discontinuity of the first and higher derivatives at the points where the segments meet, and the existence and the rationality of the angles in the boundary. Important effects appear when the concave boundary segments are introduced [7]. The focusing properties were discussed in Ref. [45].

Far from being of exclusively theoretical interest, billiards have also been the subject of extensive experimental research. Due to the equivalence of the free particle dynamics and the ray limit of the wave motion, the experiments were realized with the flat microwave and ultrasound cavities, with the light resonators and quantum dots [18,46–51]. An exemplary application of the billiard theory leading to the major technological advance is described in Ref. [51], whereby switching from the ''whispering-gallery'' orbit in the circular laser resonator to the bow-tie type of orbit in the oval-shaped resonator, the power output of the semiconductor microlaser was enhanced by three orders of magnitude.

II. THE LEMON-SHAPED BILLIARDS WITH HYPERBOLIC AND ELLIPTICAL BOUNDARY ARCS

In this paper we investigate properties of a new family of lemon-shaped billiards. Their boundaries depend on the shape parameter δ, and are described in the x-y plane by the expression

$$y = \pm \frac{\sqrt{1+\delta(\delta-2)(1-x^2)}-1}{\delta-2}, \tag{1}$$

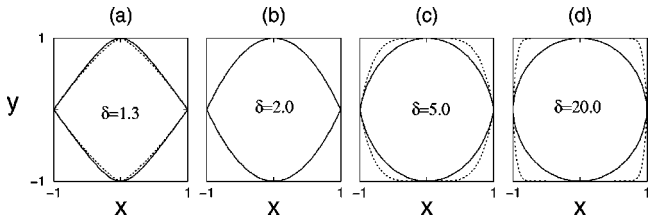

FIG. 1. The shape of the EHB billiard boundary (full line) for (a) $\delta=1.3$, (b) $\delta=2.0$, (c) $\delta=5.0$, and (d) $\delta=20.0$. The shape of the GPB billiard introduced in Ref. [52] is also shown (dotted line).

where $x\in[-1,1]$. These billiards, which we call ellipse hyperbola billiards (EHB), contain convex hyperbolic, elliptical, or parabolic arc segments, and can be considered as another extension of the convex lemon-shaped parabolic boundary

$$y=\pm(1-x^2) \tag{2}$$

first introduced in Ref. [52]. Convex parabolic and hyperbolic arcs have not been previously reported for nongravitational billiards. Except for the full elliptical billiard, which is integrable, and the elongated half-ellipses [45], there has been also no explicit reference to the convex billiards containing elliptical arcs.

The billiards (1) are inscribed into the square of side two and are shown in Fig. 1 for several values of the shape parameter δ. For $\delta=1$, the billiard is a tilted square of side $\sqrt{2}$. For $\delta=\infty$ it is the full circle, and in this limit the billiard is integrable. Also, the square limit is integrable, but many of its properties are still being investigated classically and quantally. We concentrate our attention to the billiards (1) for $1<\delta<2$, when the billiard arcs are hyperbolical, and for $2<\delta<\infty$, when the arcs are elliptical. In the limit $\delta=2$ the billiard arcs have parabolic shape described by Eq. (2). Preliminary calculations [53,54] have shown that the changes in the billiard shape influence strongly the orbit structure and the degree of chaos in the classical dynamics. These changes are reflected in the corresponding Poincaré diagrams, shown in Fig. 2 for hyperbolic and parabolic shapes in the interval $1<\delta\leqslant 2$, and in Fig. 3, where Poincaré diagrams are given for $2<\delta<\infty$, when the shape is elliptical. The angle A of the billiard (see Fig. 4) is related to the shape parameter as

$$\delta=\tan\frac{A}{2}. \tag{3}$$

The Poincaré diagrams in Figs. 2 and 3 were obtained in the following way. Instead of presenting the coordinate and the parting velocity of the particle at the bouncing point, we plot the coordinate x and the x-component $v_x=\cos\psi$ of the velocity at each point where the particle crosses the x axis (Fig. 4). The resulting plot is area conserving, while at the same time, the numerical integrations, which would be necessary for the length-of-arc Birkhoff coordinates, are avoided. The most conspicuous feature of the obtained Poincaré diagrams is a number of elliptical invariant points, surrounded by quasiregular islands, whose area, shape, and boundary change

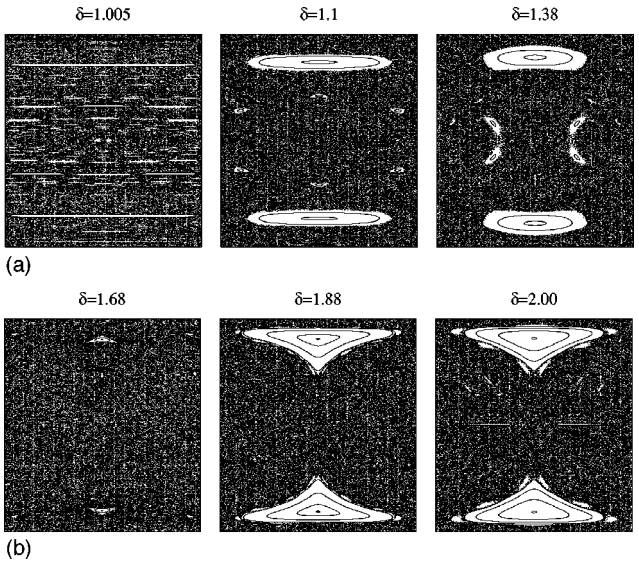

FIG. 2. Poincaré sections for the hyperbolic EHB arc shapes (a) $\delta=1.005$, (b) $\delta=1.1$, (c) $\delta=1.38$, (d) $\delta=1.68$, and (e) $\delta=1.88$, and for the parabolic arcs (f) $\delta=2.0$.

with the variation of δ. The largest of these islands reflect the existence of characteristical stable low period closed orbits.

Strong dependence on δ observed in the Poincaré diagrams is due to fluctuations in the degree of chaos and can be characterized as the ''breathing chaos'' [40]. This degree can be expressed quantitatively, by computing the fraction q_{class} of the phase plane that is filled with chaotically wandering orbits. It has been stressed [55] that such measure depends on the counting-box dimension and on the number of the phase-space points included in the computation. In our investigation, we divide the phase plane section defined by $-1<x<1$ and $-1<v_x<1$ into $N=10\,000$ rectangular boxes, and for each δ take into account $n=100\,000$ points of cross-

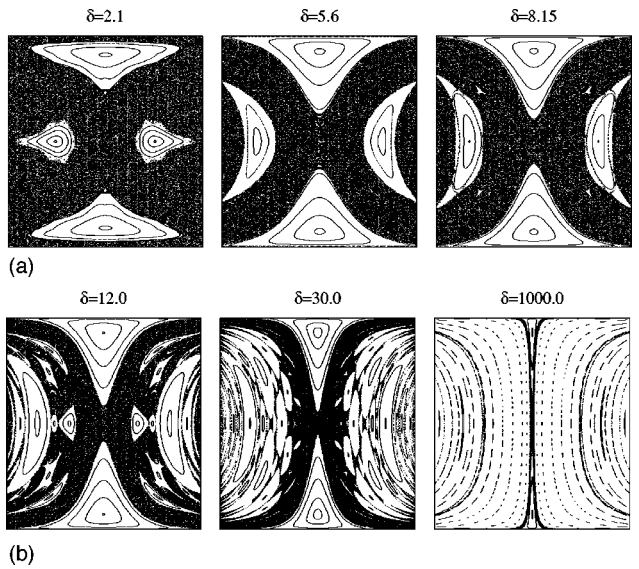

FIG. 3. Poincaré sections for the elliptical EHB arc shapes (a) $\delta=2.1$, (b) $\delta=5.6$, (c) $\delta=8.15$, (d) $\delta=12$, (e) $\delta=30$, and (f) $\delta=1000$.

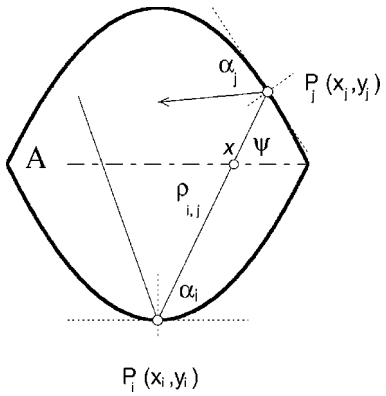

FIG. 4. Characteristic angles and orbit parameters for the particle motion in the lemon-shaped billiard.

ing the x axis. For such choice, the ratio is $n/N=10$ and the results for $q_{\rm class}$ are close to the convergence limit. The resulting $q_{\rm class}$ in dependence on δ are shown in Fig. 5. Besides the fluctuations that can be described as the ''breathing chaos,'' one notices several values of δ at which the chaotic fraction has a local maximum. We point out the maxima near $\delta=1.7$, $\delta=2.1$, $\delta=5.6$, $\delta=8.1$, $\delta=12$, and $\delta=21$, and assume that they result from some bifurcation event at the corresponding shape. For example, the maximum at $\delta=8.15$ occurs when the area of several elliptical islands (corresponding to triangular and quadrangular periodic orbits) is rapidly shrinking to negligible proportions. However, besides elliptical invariant points and their surrounding elliptical regions, the Poincaré sections for some values of δ contain singular regions, characterized by hyperbolic points. The interesting question is how these regions relate to the orbit structure and stability, and whether such points can be responsible for the sudden increase in the calculated $q_{\rm class}$ at some values of δ.

In the next few sections, we explore the properties of some billiard orbits, as follows. In Sec. III we investigate the criteria of stability for some selected orbits. Special attention is paid to two of the hyperbolic orbits and their Poincaré diagrams. Section IV is devoted to the quantum solutions for billiards (1) and to the statistical analysis of the obtained quantal spectra. In Sec. V the properties of the EHB billiard (1) are compared with those of the family of the generalized

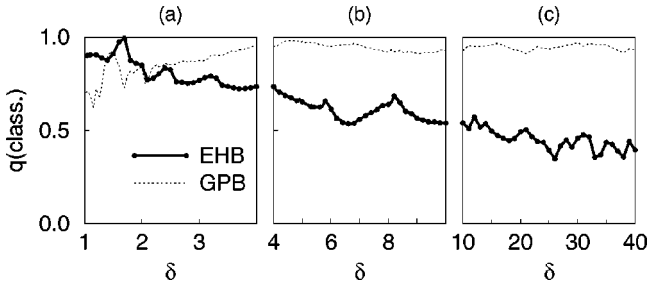

FIG. 5. Classical chaotic fraction measure $q_{\rm class}$ for the EHB billiard in dependence on δ (thick line). The corresponding result for the GPB billiard [52] is also shown (dotted line).

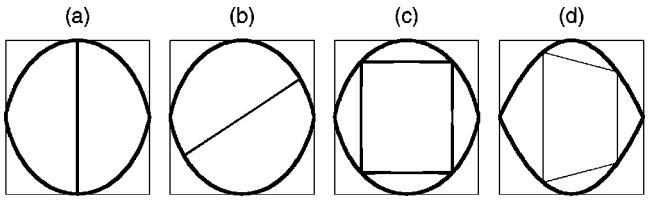

FIG. 6. Selected orbits for which the orbit stability is explored: (a) vertical two-bounce orbit, (b) tilted two-bounce orbit, (c) rectangular orbit, and (d) trapezoidal orbit typical for $\delta=2$.

power-law lemon-shaped billard family (GPB) billiards, described in Ref. [52]. Section VI contains final discussion and conclusions.

III. ANALYSIS OF STABILITY OF ORBITS AND SINGULAR REGIONS IN THE POINCARÉ DIAGRAMS

The stability of a periodic billiard orbit can be determined by computing the deviation matrix $\mathbf{M}_{n,\rm orb}$, whose trace is the criterion for stability. The orbit is stable if $|\mathbf{M}_{n,\rm orb}|<2$, unstable for $|\mathbf{M}_{n,\rm orb}|>2$, and has neutral stability if $|\mathbf{M}_{n,\rm orb}|=2$. With this method, the stability of orbits has been analyzed for a number of billiard shapes [1,7]. The deviation matrix for a periodic orbit of period n is

$$\mathbf{M}_{n,\rm orb}=\mathbf{m}_{0,n-1}\mathbf{m}_{n-1,n-2}\cdots\mathbf{m}_{2,1}\mathbf{m}_{1,0}, \tag{4}$$

where $\mathbf{m}_{i,k}$ is the matrix with unit determinant given in the Appendix. Here, we analyze the two-bounce orbits and the rectangular four-bounce orbit, as well as the special continuous family of trapezoidal orbits that occurs for $\delta=2$. Further details of the calculation of the deviation matrix are given in the Appendix.

In the EHB lemon-shaped billiards there are two types of two-bounce orbits: the vertical two-bounce orbit [Fig. 6(a)] and the tilted one [Fig. 6(b)]. Vertical has both X- and Y-reflection symmetry, as well as the central C symmetry. The tilted orbit has only the C symmetry. The rectangular orbit [Fig. 6(c)], consisting of two horizontal and two vertical segments, has X, Y, and C symmetry. In EHB billiards, all of these orbits exist in the whole range $1<\delta\leqslant\infty$.

The billiard arcs for $\delta=2$ have parabolic shape. This billiard has been discussed in Ref. [52], as a special case of the generalized power-law lemon-shaped billiard family (GPB). The special focusing property of the parabolic boundary results in a family of trapezoidal orbits. One of them is shown in Fig. 6(d). In the Poincaré sections, they are visible as two straight lines between $|x|=0.25$ and $|x|=1$ at $\nu_x=0$ [Fig. 2(f)].

In Table I, the intervals of δ in which the orbits are stable, unstable, and neutral, respectively, are given and the values of the trace of the deviation matrix in dependence on δ are also shown in Fig. 7.

The typical feature of the Poincaré sections for intermediate values of δ are large regular regions surrounding elliptical invariant points. However, at some values of the shape parameter, conspicuous is the presence of singular regions

TABLE I. Existence and stability of orbits and the traces of the corresponding deviation matrices. Symbol $d \equiv (v,h)$ stands for the direction, vertical, and horizontal, of the orbit segments, respectively. Following identities are valid: $\tau_{1d} = \sqrt{2}\rho_d/R - 1$, $\tau_{2d} = -2\rho_d$, $\tau_{3d} = \sqrt{2}/R - \rho_d/R^2$, $\rho_h = \sqrt{2(\delta-1)/\delta}$, $\delta\rho_h = (\delta-2)\rho_v + 2$, and $R = \sqrt{\delta/(\delta-1)}$.

Orbit	Existence and stability	(Tr**M**)
	2-bounce unstable	
Vertical	$1 < \delta \leqslant \infty$:	$2 + \dfrac{16\delta}{(\delta-1)^2}$
Tilted	$1 \leqslant \delta \leqslant \infty$:	$4\left[\dfrac{4(\delta-1)^2}{\delta(2\delta-1)} - 1\right]^2 - 2$
2-bounce	stable $1.236 < \delta < 2$: unstable	$6(\tau_{1h}\tau_{1v})^2 + (\tau_{2h}\tau_{3v})^2 + (\tau_{3h}\tau_{2v})^2 - 2(\tau_{1h}^2 + \tau_{1v}^2) + 4\tau_{1h}\tau_{1v}(\tau_{2v}\tau_{3h} + \tau_{3v}\tau_{2h})$
Rectangular	$\delta = 1.035, 1.236, 2, 5.068$: neutral Otherwise: stable	
Trapezoidal	$\delta = 2$: neutral	2

and singular points. Here, we discuss some details of the Poincaré sections for $\delta = 21.013$ and $\delta = 1.72\,871$.

The Poincaré section for $\delta = 21.013$ is shown in Fig. 8. Invariant points and large elliptical (KAM) regions correspond to the closed periodic orbits: two-bounce tilted orbit, some polygonal orbits (triangular, rectangular, pentagonal, hexagonal, and octogonal), and some special types of starlike orbits of periods 8, 10, and 14. Now we pay attention to the singular point situated at the position $P_5(0.3\,075\,057, 0.2\,939\,228)$. An enlarged part of the Poincaré section around this point is shown in Fig. 9(a). This is a hyperbolic point and corresponds to the motion along a five-legged star with Y symmetry, shown in Fig. 9(b). This orbit is highly unstable, as is confirmed by the calculation of the trace of the deviation matrix, which gives $\mathrm{Tr}\mathbf{M}_5 = -7.27\,009$.

An interesting feature is noticed in the Poincaré diagram for $\delta = 21.013$. The unstable hyperbolic point described

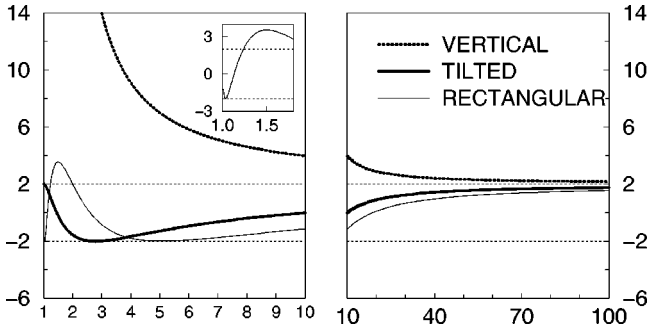

FIG. 7. The dependence on δ of the trace of the deviation matrix for the vertical two-bounce orbit (dotted thick line), tilted two-bounce orbit (full thick line), and for the rectangular orbit (full thin line).

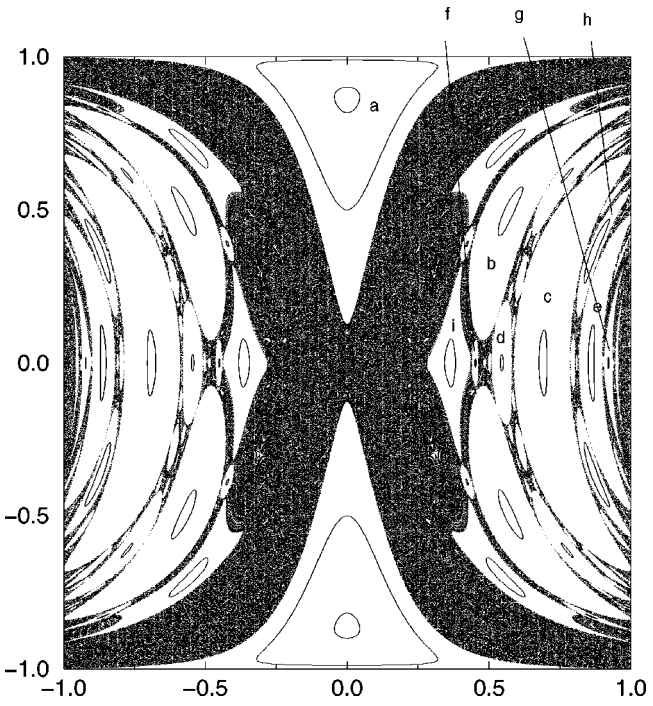

FIG. 8. The Poincaré section for $\delta = 21.013$. Invariant curves and invariant elliptical regions denoted by letters correspond to the following periodic orbits: (a) tilted two bounce, (b) triangular, (c) rectangular, (d) 10-legged star, (e) hexagonal, (f) 14-legged star, (g) octogonal, (h) pentagonal, and (i) 8-legged star.

above is surrounded by a region that has clearly the elliptical shape, although it is filled with irregularly dispersed points making part of the chaotic sea. Around a regular point one would expect a resonant belt at the border of the elliptical region. Detailed inspection of Fig. 8 shows that such resonant structure can also surround a region in whose center is a hyperbolic point. In the present case it reflects the motion of the particle along a periodic star like orbit having Y symmetry, of a very high period, shown in Fig. 9(c). The corresponding resonant belt consists of six islands, visible in Fig. 10(a). One of the six islands is shown enlarged in Fig. 10(b). It is interesting to follow this orbit around the phase plane. Its full complexity is reflected in the intricate pattern in which the orbit reappears as a part of boundary layers [Fig. 10(c)], not only of the hyperbolical point P_5, but also of several other fixed points of elliptical type.

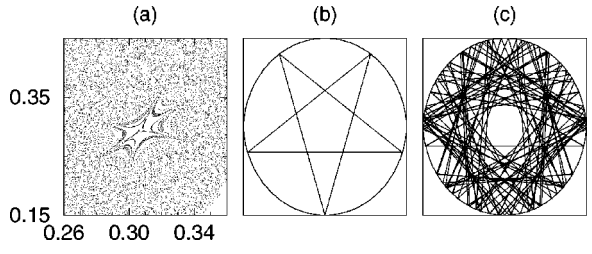

FIG. 9. (a) Strongly magnified part of the Poincaré section for $\delta = 21.013$ containing the hyperbolic point. (b) The five-legged star-like orbit responsible for the hyperbolic point shown in (a). (c) Stable periodic orbit of a high period, responsible for the belt of invariant islands surrounding the hyperbolic point shown in (a).

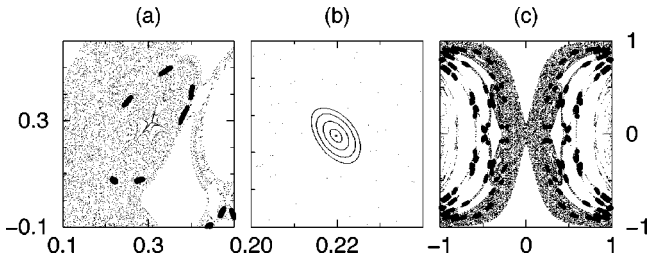

FIG. 10. (a) The belt of invariant islands corresponding to the orbit shown in Fig. 9(c). (b) The enlarged picture of the lowest lying of the six islands shown in (a). (c) The reccurrence of the invariant islands due to the orbit shown in Fig. 9(c) in different parts of the Poincaré section for $\delta=21.013$ in EHB.

Another important feature of the described singular point is illustrated in Fig. 11, where we show the enlarged portion of the singular region in the Poincaré plot for $\delta=21.013$, along with those for two neighboring values of the shape parameter. One clearly observes the inversion of the small regular triangular region revealing the existence of the 'blinking island' phenomenon, analogous to the one described for the standard map by Zaslavsky *et al.* [44].

The other example of singularity is the periodic tilted two-bounce orbit for $\delta=1.72\,871$. The corresponding Poincaré diagram is shown in Fig. 12. The hyperbolic point observed at $P_2(0,0.805\,151)$ results from the periodic tilted two-bounce orbit [Fig. 13(a)] and is surrounded by three islands, arising from the N-shaped orbit of period 6 [Fig. 13(b)]. Each of these islands has a resonant boundary layer due to the motion along the trajectory shown in Fig. 13(c). The singular point in Fig. 13 is immersed in the chaotic sea. Also in this case, the ''blinking island'' phenomenon is found (Fig. 14). Here, however, the bouncing point after 300 000 bounces still remains within the interval of the length $\Delta x=3.5\times10^{-6}$. Therefore, this orbit can be practically considered stable, as is confirmed by the calculation of the trace of the deviation matrix, which is $\mathrm{Tr}\mathbf{M}_2=0.94\,734$.

IV. THE QUANTUM BILLIARD

The billiard (1) can also be considered as a quantal system. Here we present the results of the quantum-mechanical calculations for the energy spectra. Computations of the energy spectra are based on the method of Ridell [56] for solving the Schrödinger equation

$$-\frac{\hbar^2}{2m}\nabla^2\Psi=E\Psi, \tag{5}$$

with Dirichlet boundary conditions, according to which the wave function is expanded in the basis of spherical Bessel functions of the first kind $J_\nu(kr)$ with even ν. The calculation performed for a number of values of δ in the interval $1.1<\delta<100\,000$ gives for each calculated shape an energy sequence containing between 900 and 1500 levels. The spectra obtained in this way are analyzed statistically. The calculated level spacing sequences are then unfolded by using the method of French and Wong [57]. The resulting histograms are fitted to the Brody, Berry-Robnik, and Berry-Robnik-Brody statistical distributions. The Brody [58] is an empirical distribution characterized by the parameter ω_B, which is, although lacking the fundamental explanation, widely used as a numerical value to be compared with the classical q_class. The Berry-Robnik distribution [59] depends on a single parameter q_BR, (identical to the parameter ρ_2 in [59]) and is

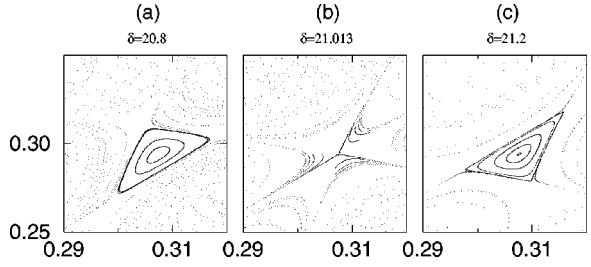

FIG. 11. Enlarged parts of the Poincaré sections for (a) $\delta=20.8$, (b) $\delta=21.013$, and (c) $\delta=21.2$, illustrating the ''blinking island'' phenomenon with the reversal of the orientation of the triangular region with the variation of δ.

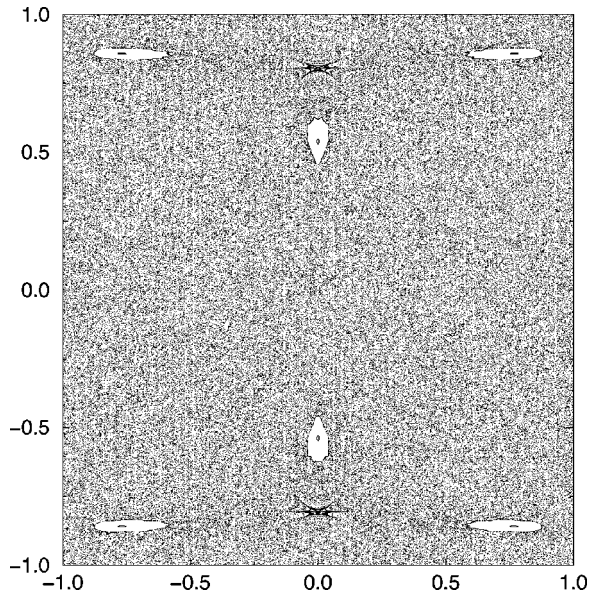

FIG. 12. The Poincaré section for $\delta=1.72\,871$. The hyperbolic and elliptical points correspond to periodic orbits shown in Fig. 13.

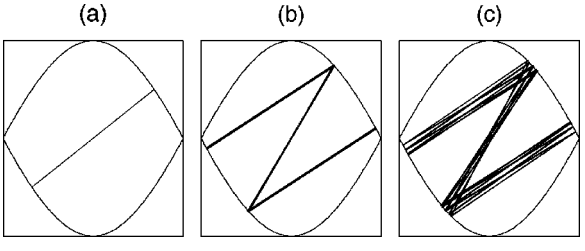

FIG. 13. (a) The tilted two-bounce orbit giving rise to hyperbolic points visible in Fig. 12. (b) The N-shaped orbit of period 6 and (c) a higher resonance of this orbit, corresponding to the elliptical islands and their resonant belts, respectively, visible in Fig. 12, for $\delta=1.72\,871$.

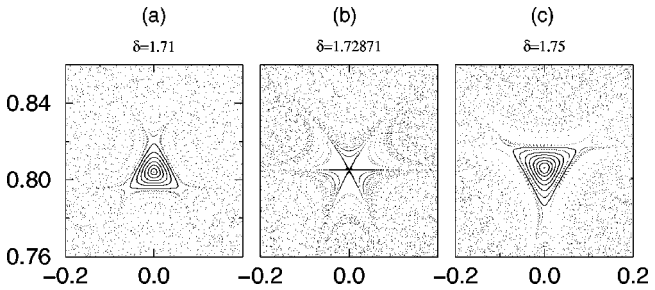

FIG. 14. Enlarged parts of the Poincaré sections for (a) $\delta=1.71$, (b) $\delta=1.72\,871$, and (c) $\delta=1.75$, illustrating the ''blinking island'' phenomenon.

considered exact in the semiclassical limit. Before the semiclassical limit is reached, more appropriate is the Berry-Robnik-Brody distribution. It depends on two parameters, q and ω, and was explicitly derived in [60]. Prosen and Robnik, who first introduced this type of the statistics in the form of the cummulative distribution [61], conclude that the parameter ω reflects the degree of localization of the wave function, whereas q is assumed to be the quantum analogue of the chaotic fraction q_{class} in the classical phase plane.

More details and definitions concerning the methods of spectrum calculations and statistical analysis can be found in [52,60]. Here we present the results of calculations for the spectra of EHB billiards. In Fig. 15(a) the values of ω_{B} for Brody distribution, q_{BR} for Berry-Robnik distribution, and q for Berry-Robnik-Brody distribution are shown in dependence on δ. The results obtained differ in absolute values, but exhibit identical fluctuations with the variation of the shape parameter δ. Results of the three statistics all show the same global behavior, having largest values around $\delta=1.7$, fluctuating for intermediate shapes $\delta\leqslant 10$, and slowly decreasing afterwards. In the interval $1<\delta\leqslant 5$, the q_{class} compare well with the Brody and Berry-Robnik results. For $\delta>5$ classical results are closer to the Berry-Robnik-Brody values of q.

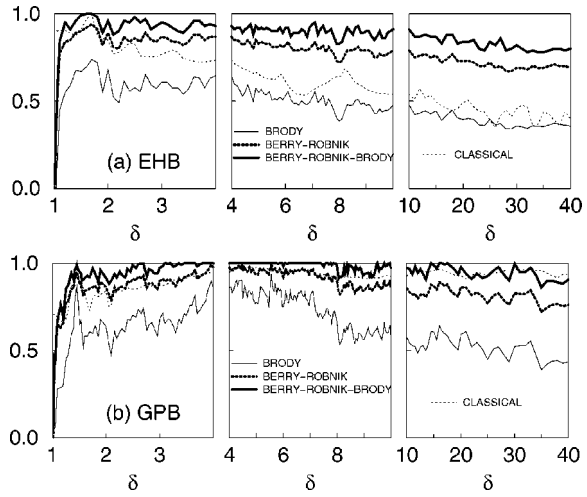

FIG. 15. Results of fitting the computed level spacings of the quantal billiard to theoretical distributions, giving the values of ω_{B} obtained with the Brody statistical distribution (full thin line), q_{BR} obtained with the Berry-Robnik statistical distribution (dotted thick line), and q obtained with the Berry-Robnik-Brody statistical distribution (full thick line), in comparison with the classical chaotic measure q_{class} (dotted thin line), in dependence on the shape parameter δ: (a) for EHB; (b) for GPB.

In an overall comparison between the classical and quantal fluctuations, there are no serious discrepancies, except near the value $\delta=8$, where the classical result exhibited a local maximum due to the bifurcation and singular points in the Poincaré diagram. This occurs probably because our quantal calculation is not able to follow all the localization effects for cases where the classical behavior is singular. It would be desirable to obtain a greater precision in the quantal calculations, and our investigations are now being extended in this direction.

V. COMPARISON OF THE ELLIPSE HYPERBOLA BILLIARD (EHB) WITH THE GENERALIZED POWER-LAW LEMON-SHAPED BILLIARD (GPB)

In Ref. [52], we have introduced the billiard family

$$y=\pm(1-|x|^{\delta}) \tag{6}$$

as the generalization of Eq. (2). This billiard we call the generalized power-law lemon-shaped billiard (GPB). The two families (1) and (6) have in common the lemonlike shape of the billiard, inscribed into the square of side 2. The lemon angle is in both families determined by the shape parameter δ as in Eq. (3). Both billiards have the same square limit when $\delta=1$, and the parabolic arc shape for $\delta=2$. They differ in the limit $\delta=\infty$, where GPB is a square and EHB is the circle. The difference of shapes is visible in Fig. 1. As δ approaches ∞, the EHB billiards are more similar to the circle, while the GPB billiards resemble to a billiard of the stadium type, owing to two nearly straight parallell-situated boundary segments. Dynamically, these differences are reflected in the existence of the eight most elemental low-period orbits, those determined by a single bouncing point. While in EHB only four of them (the tilted two-bounce, triangular, rectangular and hexagonal) exist, in GPB also the remaining four (''bird,'' ''bow-tie,'' ''hour glass,'' and ''candy-shaped'' orbit) contribute significantly [53,54].

Another comparison may be of interest, concerned with the description of the billiard boundary in the polar coordinates φ and r. The equation for the EHB reads

$$r^2(\delta-2\sin^2\varphi)+2r|\sin\varphi|-\delta=0, \tag{7}$$

giving the solution

$$r=\frac{\sqrt{(\delta-1)^2+(2\delta-1)\cos^2\varphi}-\sqrt{1-\cos^2\varphi}}{(\delta-2)+2\cos^2\varphi}, \tag{8}$$

which may be readily used with the numerical algorithms based on the polar coordinates [62]. The equation for GPB is

$$r^{\delta}|\cos\varphi|^{\delta}+r|\sin\varphi|-1=0 \tag{9}$$

and has no explicit general solution, therefore the methods designed for polar coordinates cannot be directly applied.

In Fig. 15(b) we show for GPB the results for q_{class} and the corresponding values of ω_{B}, q_{BR}, and q, obtained by fitting the calculated spectral level densities to the Brody, Berry-Robnik, and Berry-Robnik-Brody level spacing distributions, respectively. This figure should be compared with the corresponding Fig. 15(a) for EHB. For direct comparison of q_{class} in two types of billiards, in Fig. 5 we have also plotted the values q_{class} obtained for GPB.

VI. DISCUSSION AND CONCLUSIONS

In sumarizing the results presented in the previous sections, we stress the following conclusions. The billiard family (EHB) examined in our paper offers a new possibility of transition from the square billiard to the circular billiard. Examining the classical parameters describing the chaotic fraction in dependence on the shape parameter, one discovers the ''breathing chaos'' phenomenon, with local maxima in the classical value of the characteristic parameter q_{class} at some shapes. Those are connected with the singular regions and hyperbolic points occuring in the Poincaré diagrams, corresponding to selected orbits. They are hyperbolic and generaly unstable, but can be practically considered stable if the transport is extremely slow. The examination of the criteria of stability was performed for selected cases, and confirms this conclusion. Such points exhibit the special property called the ''blinking island'' phenomenon, observed previously in some nonbilliard Hamiltonian systems.

The quantum billiards with the same boundary have been investigated, resulting in the quantum analogues of the value of chaotic fraction q_{class} for EHB, obtained by fitting the calculated spectral fluctuations to the Brody, Berry-Robnik, and Berry-Robnik-Brody level spacing distributions. All three distributions exhibit the same type of fluctuations, although, as has been previously known, the absolute values cannot be expected to be the same.

Finally, we compared the results for the EHB billiards with those for the GPB billiards considered in Ref. [52]. They have in common the lemonlike shape and are both inscribed into the square of side 2. The shape parameter in both is connected with the billiard angle in the same way. In EHB, a smaller number of orbit types contributes significantly to large regular regions, especially for $\delta>2$ where the boundaries are elliptical. In GPB more orbits appear, but they are less stable and contribute to the chaotic fraction in the phase plane. For $\delta>2$, this results in q_{class} values conspicuously larger in GPB then in EHB, thus, generally, GPB billiards are more chaotic than EHB billiards with the elliptical boundary arcs. For hyperbolic arcs $1<\delta<2$, the q_{class} values oscillate, and the comparison depends strongly on the details of the shape. The overall agreement between classical and quantal q_{class} values is satisfactory, but for more precise comparison the improved computations of the energy spectra would be beneficial.

It was not possible to establish a direct connection between the billiard angle and the appearance of bifurcations and singularities in the Poincaré diagrams. It is however worth mentioning that in the EHB billiards a significant singularity appears for the shape parameter $\delta=1.72\,871$, which closely, but not precisely, corresponds to the billiard angle $A=2\pi/3$.

ACKNOWLEDGMENTS

Discussions with A. Bjeliš, V. Dananić, H. Makino, and M. Robnik are gratefully acknowledged.

APPENDIX

The deviation matrix for a periodic orbit is given by expression (4), where $\mathbf{m}_{i,k}$ is the matrix with unit determinant [1]

$$\mathbf{m}_{i,k}=\begin{pmatrix} -\dfrac{\sin(\alpha_i)}{\sin(\alpha_k)}+\dfrac{\rho_{i,k}}{\sin(\alpha_k)R_i} & -\dfrac{\rho_{i,k}}{\sin(\alpha_i)\sin(\alpha_k)} \\ -\dfrac{\rho_{i,k}}{R_iR_k}+\dfrac{\sin(\alpha_k)}{R_i}+\dfrac{\sin(\alpha_i)}{R_k} & -\dfrac{\sin(\alpha_k)}{\sin(\alpha_i)}+\dfrac{\rho_{i,k}}{\sin(\alpha_i)R_k} \end{pmatrix}. \tag{A1}$$

The symbol R_i denotes the curvature radius at the bouncing point $P_i(x_i,y_i)$

$$R_i=\frac{[(\delta-1)^2+2\delta x_i^2]^{3/2}}{\delta(\delta-1)^2}, \tag{A2}$$

$\rho_{i,k}$ is the length of the orbit segment between the bouncing points P_i and P_k, and α_i is the angle which the departing orbit closes with the tangent on the billiard boundary at the bouncing point P_i (Fig. 4).

For the two-bounce orbits the deviation matrix is

$$\mathbf{M}_2=(\mathbf{m}_{0,1})^2. \tag{A3}$$

Both bouncing angles are $\alpha=\pi/2$. The lenght of the segments is $\rho=2$ for the vertical, and $\rho=\sqrt{2(2\delta-1)/\delta}$ for the tilted two-bounce orbit. The curvature radius is $R=(\delta$

$-1)/\delta$ for the vertical and $R=(2\delta-1)[2\delta(2\delta-1)]^{1/2}/[4(\delta-1)^2]$ for the tilted orbit.

The deviation matrix for the rectangular orbit is

$$\mathbf{M}_{4,\mathrm{rect}}=(\mathbf{m}_{2,1}\mathbf{m}_{1,0})^2. \tag{A4}$$

All four bouncing angles are $\alpha=\pi/4$. The curvature radius for all bouncing points is $R=\sqrt{\delta/(\delta-1)}$, and the lenghts of the horizontal and vertical segments, respectively, are $\rho_h=\sqrt{2(\delta-1)/\delta}$ and $\rho_v=[\sqrt{2\delta(\delta-1)}-2]/(\delta-2)$. The deviation matrix for the trapezoidal orbit for $\delta=2$ is

$$\mathbf{M}_{4,\mathrm{trap}}=\mathbf{m}_{0,3}\mathbf{m}_{3,2}\mathbf{m}_{2,1}\mathbf{m}_{1,0}. \tag{A5}$$

This orbit is characterized by coordinates x_0 and $-1/x_0$, with $0.25\leqslant|x_0|\leqslant 1$. The sinuses of the bouncing angles are $\sin(\alpha_0)=\sin(\alpha_3)=1/(1+4x_0^2)$ and $\sin(\alpha_1)=\sin(\alpha_2)=2x_0/(1+4x_0^2)$. The curvature radiuses are $R_0=R_3=(1-4x_0^2)^{3/2}/2$ and $R_1=R_2=(1-4x_0^2)^{3/2}/(16x_0^3)$. The orbit segments are $\rho_{0,1}=\rho_{2,3}=[(1/4x_0^2)+x_0]^2$, $\rho_{1,2}=2(1-x_0^2)$, and $\rho_{3,0}=2-(1/8x_0^2)$.

[1] M. Berry, Eur. J. Phys. **2**, 91 (1981).
[2] G. Benettin and J. M. Strelcyn, Phys. Rev. A **17**, 773 (1978).
[3] Ya. G. Sinai, Russ. Math. Surv. **25**, 137 (1979).
[4] S. W. McDonald and A. N. Kaufman, Phys. Rev. Lett. **42**, 1189 (1979).
[5] O. Bohigas, M. J. Giannoni, and C. Schmit, Phys. Rev. Lett. **52**, 1 (1984).
[6] E. J. Heller and S. Tomsovic, Phys. Today **46(7)**, 38 (1993).
[7] H. R. Dullin, P. H. Richter, and A. Wittek, Chaos **6**, 43 (1996).
[8] A. Hayli and Th. Dumont, Celest. Mech. **38**, 23 (1986).
[9] F. Leyvraz, C. Schmit, and T. H. Seligman, J. Phys. A **29**, L575 (1996).
[10] H. Makino, T. Harayama, and Y. Aizawa, Phys. Rev. E **59**, 4026 (1999).
[11] T. Prosen, J. Phys. A **31**, 7023 (1998).
[12] M. Robnik, J. Phys. A **16**, 3971 (1983).
[13] A. Bäcker, F. Steiner, and P. Stifter, Phys. Rev. E **52**, 2463 (1995).
[14] A. Bäcker and H. R. Dullin, J. Phys. A **30**, 1991 (1997).
[15] M. Robnik, J. Dobnikar, and T. Prosen, J. Phys. A **32**, 1427 (1999).
[16] M. Jeng and O. Knill, Chaos, Solitons Fractals **7**, 543 (1996).
[17] R. Aurich, T. Hesse, and F. Steiner, Phys. Rev. Lett. **74**, 4408 (1995).
[18] H. Alt, H.-D. Gräf, H. L. Harney, R. Hofferbert, H. Lengeler, C. Rangacharyulu, A. Richter, and P. Schardt, Phys. Rev. E **50**, R1 (1994).
[19] J. Ma and K. Nakamura, Phys. Rev. B **60**, 10 676 (1999).
[20] G. Veble, M. Robnik, and J. Liu, J. Phys. A **32**, 6423 (1999).
[21] E. J. Heller and P. W. O'Connor, Nucl. Phys. B (Proc. Suppl.) **2**, 201 (1987).
[22] M. Sieber, U. Smilansky, S. C. Creagh, and R. G. Littlejohn, J. Phys. A **26**, 6217 (1993).
[23] H. D. Parab and S. R. Jain, J. Phys. A **29**, 3903 (1996).
[24] M. Robnik and T. Prosen, J. Phys. A **30**, 8787 (1997).
[25] F. P. Simonotti, E. Vergini, and M. Saraceno, Phys. Rev. E **56**, 3859 (1997).
[26] M. Robnik, Nonl. Phen. Compl. Sys. **1**, 1 (1998).
[27] D. Biswas, Phys. Rev. E **54**, R1044 (1996).
[28] R. Artuso, G. Casati, and I. Guarneri, Phys. Rev. E **55**, 6384 (1997).
[29] G. Casati and T. Prosen, Phys. Rev. Lett. **83**, 4729 (1999).
[30] M. Robnik and G. Veble, J. Phys. A **31**, 4669 (1998).
[31] R. D. Connors and J. P. Keating, J. Phys. A **25**, 555 (1999).
[32] A. J. S. Traiber, A. J. Fendrik, and M. Bernath, J. Phys. A **23**, L305 (1990).
[33] D. K. Siegwart, J. Phys. A **22**, 3537 (1989).
[34] M. Robnik and M. V. Berry, J. Phys. A **18**, 1361 (1985).
[35] H. Frisk and R. Arvieu, J. Phys. A **22**, 1765 (1989).
[36] S. Borgan and R. C. Johnson, Phys. Lett. A **262**, 427 (1999).
[37] H. E. Lehtihet and B. N. Miller, Physica D **21**, 93 (1986).
[38] T. Szeredi and D. A. Goodings, Phys. Rev. E **48**, 3518 (1993).
[39] T. Szeredi and D. A. Goodings, Phys. Rev. E **48**, 3529 (1993).
[40] P. H. Richter (unpublished).
[41] P. H. Richter, H.-J. Scholz, and A. Wittek, Nonlinearity **3**, 45 (1990).
[42] H. J. Korsch and J. Lang, J. Phys. A **24**, 45 (1991).
[43] M. L. Ferguson, B. N. Miller, and M. A. Thompson, Chaos **9**, 841 (1999).
[44] G. M. Zaslavsky, M. Edelman, and B. A. Nyazov, Chaos **7**, 159 (1996).
[45] V. J. Donnay, Commun. Math. Phys. **141**, 225 (1991).
[46] J. Stein and H. J. Stöckmann, Phys. Rev. Lett. **68**, 2867 (1992).
[47] S. Sridhar and E. J. Heller, Phys. Lett. A **46**, R1728 (1992).
[48] A. D. Stone and H. Bruus, Physica B **189**, 43 (1993).
[49] P. A. Chinnery and V. F. Humphrey, Phys. Rev. E **53**, 272 (1996).
[50] J. A. Katine, M. A. Eriksson, A. S. Adourian, R. M. Westerwelt, J. D. Edwards, A. Lupusaux, E. J. Heller, R. M. Campman, and A. C. Goshard, Phys. Rev. Lett. **79**, 4806 (1997).
[51] C. Gmachl, F. Capasso, E. E. Narimanov, J. U. Nöckel, A. D. Stone, J. Faist, D. L. Sivco, and A. Y. Cho, Science **280**, 1564 (1998).
[52] V. Lopac, I. Mrkonjić, and D. Radić, Phys. Rev. E **59**, 303 (1999).
[53] V. Lopac, Adv. Ser. Astrophys. Cosmology **10**, 609 (1999).
[54] I. Mrkonjić, D. Radić, V. Dananić, and V. Lopac, Prog. Theor. Phys. Suppl. **139**, 382 (2000).
[55] T. Prosen and M. Robnik, J. Phys. A **31**, L345 (1998).
[56] R. J. Ridell, Jr., J. Comput. Phys. **31**, 21 (1979).
[57] J. B. French and S. S. M. Wong, Phys. Lett. **35B**, 5 (1971).
[58] T. A. Brody, Lett. Nuovo Cimento **7**, 482 (1973).
[59] M. V. Berry and M. Robnik, J. Phys. A **17**, 2413 (1984).
[60] V. Lopac, S. Brant, and V. Paar, Z. Phys. A **356**, 113 (1996).
[61] T. Prosen and M. Robnik, J. Phys. A **27**, 8059 (1994).
[62] H. J. Korsch and H.-J. Jodl, *Chaos* (Springer-Verlag, Berlin, 2000).